Numerical Simulation of the Evolution of Wound Healing in the 3D Environment

J. N. Nchejane [a*], S. O. Gbenro [b] and M. E. Thakedi [a]

[a] *Department of Mathematics and Computer Science, National University of Lesotho, Lesotho.*
[b] *Department of Mathematical Science, Bamidele Olumilua University of Education, Science and Technology, Ikere-Ekiti, Nigeria.*

Authors' contributions

This work was carried out in collaboration among all authors. All authors read and approved the final manuscript.

Article Information

Original Research Article

Abstract

Numerical simulation of the wound healing behaviour by considering the coupled reaction-diffusion, transport and viscoelastic system is vital in investigating the mechanical stress field induced by cell migration. In this work, numerical simulation is viewed in three-dimensional space during a time course of wound healing. Over the years, many authors have developed two-dimensional mathematical models of wound healing, as supported by the background in the introduction below. But we know that a three-dimensional case realistically captures the tissue deformations. The two-dimensional simulation is restricted to observing the motion in two directions only. Hence, the interest is in the three-dimensional case. Therefore, to our knowledge, this is the first article to consider the numerical simulation of the coupled reaction-diffusion, transport and viscoelastic system during wound healing in a three-dimensional environment. Firstly, the two-dimensional evolution of wound healing is developed to compare our results with published data. Then the work is extended to three-dimensional wound healing, which is the main focus.

Keywords: Numerical simulation; wound healing; reaction-diffusion; cell migration; viscoelastic system.

_____

*Corresponding author: Email: jn.nchejane@nul.ls;

1 Introduction

Wound healing is a complex phenomenon. Different authors model this healing process differently by considering specific parameters while ignoring other parameters from the mathematical point of view. Parameters mainly utilized involve extracellular matrix, wound contraction, cell traction, and angiogenesis [1-6]]. McDougall, Dallon [7] developed a mathematical model of fibroblast cell migration and collagen deposition following a dermal wound. Due to the chemoattractant gradient, it was found that fibroblasts move rapidly into the damaged tissue to replace the dead cells. Furthermore, this study revealed how the complex wound structure is affected during wound healing.

Murray and Oster [8] developed a one-dimensional case of coupled reaction-diffusion, transport and viscoelastic systems and studied cell traction to create patterns and form in morphogenesis. This was the first study to derive this system from studying morphogenesis during wound healing. These equations were also put in the proper form by performing non-dimensionalization. Murray and Oster also developed other models to study cell traction to establish patterns and structure in morphogenesis in the evolution of wound healing. Later, Sherratt, Martin [9] developed mathematical models to account for wound healing in embryonic and adult epidermis. They studied the mechanisms of epidermal repair in embryos and adults. Furthermore, they accounted for actin alignment during embryonic wound healing using the mechanical model. In contrast, reaction-diffusion was used to find the impact of growth factors during wound healing in adults. In 1994, Dale, Maini [2] proposed a reaction-diffusion model to study the mechanisms involved in healing corneal surface wounds. This study found that some of their solutions for cell density and epidermal growth factors evolved into travelling waves, while others failed to develop into travelling waves.

Cumming, McElwain [10] investigated the role of the cytokine transforming growth factor-beta during the healing and scar development using the mathematical model. This model reveals the history of using the reaction-diffusion equation to model processes involved during wound healing. It was also found in the same paper that fibroblasts quickly populate the wound within four days following the injury to the tissue in response to the chemotactic gradient. Several models on wound healing using the reaction-diffusion equation have been well documented [11]. These include epidermis and dermis damage models, chronic disorders and solid tumour growth. Jorgensen and Sanders [12] gave a comprehensive review of the advances in mathematical modelling of wound healing and wound closure. These models include only investigate the biomechanics of the tissue during the wound healing process [13-16]]. Another great review of computational wound healing models was previously carried out [17].

Recently, agent-based modelling has been adopted to model the dynamics involved during wound healing. One such model was developed to investigate how fibroblasts integrate local chemical, structural, and mechanical cues as they deposit and remodel collagen [18]. This model represented a section of the heart myocardium perpendicular to the epicardial surface on the heart's left ventricle. Later, this model was coupled with the finite element model to get realistic deformations from the finite element model to drive the agent-based model [19].

The current study focuses on skin wound healing, modelled by a coupled system of reaction-diffusion, transport and viscoelastic equations. This system is solved numerically using finite difference schemes. We began by solving the two-dimensional case compared with previously published data. Then this model is extended to a three-dimensional case.

2 The Governing Model

2.1 Two-dimensional Case

The wound healing model consists of the following system of equations.

$$\frac{\partial n}{\partial t} + \frac{\partial}{\partial x}\left[n\frac{\partial u}{\partial t} + \chi(\rho)n\frac{\partial \rho}{\partial x} - D(\rho)\frac{\partial n}{\partial x}\right] = P(n,\rho),$$
$$\frac{\partial \rho}{\partial t} + \frac{\partial}{\partial x}\left(\rho\frac{\partial u}{\partial t}\right) = B(n,\rho), \quad (1)$$
$$\frac{\partial}{\partial x}\left[n\frac{\partial^2 u}{\partial x \partial t} + E\frac{\partial u}{\partial x} + \tau(n,\rho)\right] = F(u,\rho),$$

where,

- $\rho(x,t)$ is the extracellular matrix (ECM) density
- n is the cell density
- u is the displacement
- $D(\rho)$ with constant diffusion coefficient
- $\chi(\rho)$ is the chemotaxis with chemotactic sensitivity
- $\mathbf{B(n,\rho)}$ represents ECM biosynthesis and degradation
- Body forces, $F(u,\rho) = su\rho$, measure the ECM matrix's strength to the underlying tissues.

Generally, the ECM matrix is attached elastically to the epithelial layer. The body force, $F(u,\rho)$, is assumed to be due to external tethering to the basement membrane and modelled by a linear spring, where s is a constant of proportionality.

Traction forces depend on the adhesion between the cell surface and collagen fibres.

$$\tau(n,\rho) = \frac{T_0 n\rho}{R^2 + \rho^2},\tag{2}$$

where T_0 and R are constant parameters as previously found by numerical simulation [20,21]

The following assumptions we used in this model:

- We set the cell and the ECM density to one for normal tissue.
- Fibroelastic cells proliferate according to a logistic growth law,

$$P = rn(1-n),$$

where r is the linear growth rate and $r > 0$.

- Set D>0 as a constant.
- The collagen biosynthesis and degradation rate are assumed to be proportional to n and $-np$.

$$B = \epsilon n(1-p),$$

- and where ε is very small to introduce the fact that the ECM remodelling takes more time than the proliferation of cells.
- The positive parameters μ and E quantify the viscous and elastic contributions.
- We neglect haptotactic contributions.

The following boundary conditions we utilized around the wound domain:

$$\frac{\partial n}{\partial x}(0,t) = \frac{\partial \rho}{\partial x}(0,t) = u(0,t) = 0,$$
$$n(\infty,t) = \rho(\infty,t) = 1,$$
$$u(\infty,t) = 0,\tag{3}$$

with the initial conditions given by

$$n(x,0) = H(x-1),$$
$$\rho(x,0) = \rho_i + (1-\rho_i)H(x-1)\tag{4}$$
$$u(x,0) = 0,$$

where H is the Heaviside functions.

2.2 Three-dimensional Case

The same system was upgraded to a two-dimensional case as given below

$$\frac{\partial n}{\partial t} + \text{div}\left[n\frac{\partial \mathrm{u}}{\partial t} + \chi(\rho)n\nabla\rho - D(\rho)\nabla n\right] = P(n,\rho)$$

$$\frac{\partial \rho}{\partial t} + \text{div}\left(\rho\frac{\partial \mathrm{u}}{\partial t}\right) = B(n,\rho)$$

$$-\text{div}\left[\mu\frac{\partial(\nabla \mathrm{u})}{\partial t} + E\nabla \mathrm{u} + \tau(n,\rho)I\right] + F(n,\rho) = 0 \tag{5}$$

We now divide the displacement in u_1 and u_2 for the movement in x and y direction, respectively:

$$\frac{\partial n}{\partial t} + \frac{\partial}{\partial x}\left[n\frac{\partial u_1}{\partial t} + \chi(\rho)n\frac{\partial \rho}{\partial x} - D(\rho)\frac{\partial n}{\partial x}\right] + \frac{\partial}{\partial y}\left[n\frac{\partial u_2}{\partial t} + \chi(\rho)n\frac{\partial \rho}{\partial y} - D(\rho)\frac{\partial n}{\partial y}\right] = P(n,\rho),$$

$$\frac{\partial \rho}{\partial t} + \frac{\partial}{\partial x}\left(\rho\frac{\partial u_1}{\partial t}\right) + \frac{\partial}{\partial y}\left(\rho\frac{\partial u_2}{\partial t}\right) = B(n,\rho),$$

$$-\left[\mu\begin{pmatrix}\frac{\partial(\Delta u_1)}{\partial t}\\\frac{\partial(\Delta u_2)}{\partial t}\end{pmatrix} + E\begin{pmatrix}\Delta u_1\\\Delta u_2\end{pmatrix} + \begin{pmatrix}\frac{\partial \tau}{\partial x}\\\frac{\partial \tau}{\partial y}\end{pmatrix}\right] + F(n,\rho) = 0, \tag{6}$$

with the following boundary conditions and the same assumptions used in the two-dimensional case were also applied in the three-dimensional environment:

$$n(x,0,t) = n(x,\infty,t) = \rho(x,0,t) = \rho(x,\infty,t) = 1,$$

$$\frac{\partial n}{\partial x}(0,y,t) = \frac{\partial n}{\partial x}(\infty,y,t) = \frac{\partial \rho}{\partial x}(0,y,t) = \frac{\partial \rho}{\partial x}(\infty,y,t) = 0,$$

$$u(x,0,t) = u(x,\infty,t) = u(0,y,t) = u(\infty,y,t) = 0. \tag{7}$$

3 Finite difference scheme

We apply the implicit finite difference on the spatial variable and the Euler scheme for the time variable in the following sections. It has already been proved that an implicit scheme converges, and it is stable unconditionally [22,23]].

3.1 Three-dimensional case

We use forward or backward Euler depending on the direction of the flow.

If $\frac{\partial u}{\partial t} < 0$ we have;

$$C = \frac{n_{i+1}^N(u_{i+1}^{N+1} - u_{i+1}^N) - n_i^N(u_i^{N+1} - u_i^N)}{dx},$$

$$A = \frac{\rho_{i+1}^N(u_{i+1}^{N+1} - u_{i+1}^N) - \rho_i^N(u_i^{N+1} - u_i^N)}{dx}.$$

If $\frac{\partial u}{\partial t} > 0$ we have

$$C = \frac{n_i^N(u_i^{N+1} - u_i^N) - n_{i-1}^N(u_{i-1}^{N+1} - u_{i-1}^N)}{dx},$$

$$A = \frac{\rho_i^N(u_i^{N+1} - u_i^N) - \rho_{i-1}^N(u_{i-1}^{N+1} - u_{i-1}^N)}{dx}.$$

Substituting all the above discrete forms into equation **(1)** and discretizing the remaining terms, we get:

$$n_i^{N+1} = n_i^N - C - \frac{\chi_i n_i dt\left(\rho_{i+1}^N - \rho_i^N\right) - \chi_{i-1} n_{i-1} dt\left(\rho_i^N - \rho_{i-1}^N\right)}{dx^2} + \frac{D_i dt\left(n_{i+1}^N - n_i^N\right) - D_{i-1} dt\left(n_i^N - n_{i-1}^N\right)}{dx^2} + dt P(n,\rho)_i,$$

$$\rho_i^{N+1} = \rho_i^N - A + B(n,\rho)_i,$$

$$\left(\frac{\mu}{dt} + E\right)\left(\frac{-u_{i+1}^{N+1} + 2u_i^{N+1} - u_{i-1}^{N+1}}{dx^2}\right) + F_i = \frac{\mu}{dt}\left(\frac{-u_{i+1}^N + 2u_i^N - u_{i-1}^N}{dx^2} + \frac{\tau_{i+1}^N - \tau_i^N}{dx}\right),$$

where $F_i = s\rho_i^N u_i^{N+1}$. (8)

The above discrete equations result in algebraic equations, which can be turned into a matrix form. Considering only the last equation in (8), we get the following matrix form of the equations:

$$\left(\frac{\mu}{dt} + E\right) Bu^{N+1} = \frac{\mu}{dt} B_1 u^N + \tau^N. \tag{9}$$

Below is an example of the form of the tridiagonal matrix from B:

$$\frac{1}{dx^2}\begin{pmatrix} 2 & -1 & 0 & \cdots & 0 \\ -1 & 2 & -1 & \ddots & \vdots \\ 0 & \ddots & \ddots & \ddots & 0 \\ \vdots & \ddots & -1 & 2 & -1 \\ 0 & \cdots & 0 & -1 & 2 \end{pmatrix}.$$

3.2 Two-dimensional case

In the following, we derive the discrete form of the time derivate, which is dependent on the flow direction or direction of the migration of the cells within the wound.

Flow: x direction

If $\frac{\partial u_1}{\partial t} < 0$ we have:

$$C_1 = \frac{n_{i+1,j}^N\left(u_{1(i+1,j)}^{N+1} - u_{1(i+1,j)}^N\right) - n_{i,j}^N\left(u_{1(i,j)}^{N+1} - u_{1(i,j)}^N\right)}{dx},$$

$$G_1 = \frac{\rho_{i+1,j}^N\left(u_{1(i+1,j)}^{N+1} - u_{1(i+1,j)}^N\right) - \rho_{i,j}^N\left(u_{1(i,j)}^{N+1} - u_{1(i,j)}^N\right)}{dx}.$$

If $\frac{\partial u_1}{\partial t} > 0$ we have:

$$C_1 = \frac{n_{i,j}^N\left(u_{1(i,j)}^{N+1} - u_{1(i,j)}^N\right) - n_{i-1,j}^N\left(u_{1(i-1,j)}^{N+1} - u_{1(i-1,j)}^N\right)}{dx},$$

$$G_1 = \frac{\rho_{i,j}^N\left(u_{1(i,j)}^{N+1} - u_{1(i,j)}^N\right) - \rho_{i-1,j}^N\left(u_{1(i-1,j)}^{N+1} - u_{1(i-1,j)}^N\right)}{dx}.$$

Flow: y direction

If $\frac{\partial u_2}{\partial t} < 0$ we have:

$$C_2 = \frac{n_{i,j+1}^N\left(u_{2(i,j+1)}^{N+1} - u_{2(i,j+1)}^N\right) - n_{i,j}^N\left(u_{2(i,j)}^{N+1} - u_{2(i,j)}^N\right)}{dy},$$

$$G_2 = \frac{\rho_{i,j+1}^N\left(u_{2(i,j+1)}^{N+1} - u_{2(i,j+1)}^N\right) - \rho_{i,j}^N\left(u_{2(i,j)}^{N+1} - u_{2(i,j)}^N\right)}{dy}.$$

If $\frac{\partial u_2}{\partial t} > 0$ we have:

$$\frac{n_{i,j}^N \left(u_{2(i,j)}^{N+1} - u_{2(i,j)}^N \right) - n_{i,j-1}^N \left(u_{2(i,j-1)}^{N+1} - u_{2(i,j-1)}^N \right)}{dy},$$

$$G_2 = \frac{\rho_{i,j}^N \left(u_{2(i,j)}^{N+1} - u_{2(i,j)}^N \right) - \rho_{i,j-1}^N \left(u_{2(i,j-1)}^{N+1} - u_{2(i,j-1)}^N \right)}{dy}.$$

Again plugging in the above equations in (6) and discretizing the remaining terms, we get:

$$n_{i,j}^{N+1} = n_{i,j}^N - C_1 \frac{dt \left(\chi_{i,j}^N n_{i,j} \left(\rho_{i+1,j}^N - \rho_{i,j}^N \right) - \chi_{i-1,j}^N n_{i-1,j} \left(\rho_{i,j}^N - \rho_{i-1,j}^N \right) \right)}{dx^2} + \frac{dt \left(D_{i,j}^N \left(n_{i+1,j}^N - n_{i,j}^N \right) - D_{i-1,j}^N \left(n_{i,j}^N - n_{i-1,j}^N \right) \right)}{dx^2}$$

$$- C_2 \frac{dt \left(\chi_{i,j}^N n_{i,j}^N \left(\rho_{i,j+1}^N - \rho_{i,j}^N \right) - \chi_{i,j-1}^N n_{i,j-1}^N \left(\rho_{i,j}^N - \rho_{i,j-1}^N \right) \right)}{dy^2} +$$

$$\frac{dt \left(D_{i,j}^N \left(n_{i,j+1}^N - n_{i,j}^N \right) - D_{i,j-1}^N \left(n_{i,j}^N - n_{i,j-1}^N \right) \right)}{dy^2} + dt P_{i,j}^N \rho_{i,j}^{N+1} = \rho_{i,j}^N - G_1 - G_2 + dt B_{i,j}^N \tag{10}$$

$$\left(\frac{\mu}{dt} + E \right) \left(\frac{u_{1i+1,j}^{N+1} - 2u_{1i,j}^{N+1} + u_{1i-1,j}^{N+1}}{dx^2} + \frac{u_{1i,j+1}^{N+1} - 2u_{1i,j}^{N+1} + u_{1i,j-1}^{N+1}}{dy^2} \right) + F_{1i,j}^{N+1} = \frac{-\mu}{dt} \left(\frac{u_{1i+1,j}^N - 2u_{1i,j}^N + u_{1i-1,j}^N}{dx^2} + \right.$$
$$\left. u1_{i,j+1}^N - 2u1_{i,j}^N + u1_{i,j-1}^N dy2 + \tau_{i+1,j}^N - \tau_{i,j}^N dx \right. \tag{11}$$

$$- \left(\frac{\mu}{dt} + E \right) \left(\frac{u_{2i+1,j}^{N+1} - 2u_{2i,j}^{N+1} + u_{2i-1,j}^{N+1}}{dx^2} + \frac{u_{2i,j+1}^{N+1} - 2u_{2i,j}^{N+1} + u_{2i,j-1}^{N+1}}{dy^2} \right) + F_{2i,j}^{N+1} = -\frac{\mu}{dt} \left(\frac{u_{2i+1,j}^N - 2u_{2i,j}^N + u_{2i-1,j}^N}{dx^2} + \right.$$
$$\left. \frac{u_{2i,j+1}^N - 2u_{2i,j}^N + u_{2i,j-1}^N}{dy^2} \right) + \frac{\tau_{i,j+1}^N - \tau_{i,j}^N}{dy} \tag{12}$$

The above equations result in an algebraic system of equations, which can be written in a compact matrix form. In the following, we give an example of what equation (12) will look like in the compact matrix form:

$$\left(\frac{\mu}{dt} + E \right) A_1 u_1^{N+1} = \frac{\mu}{dt} A_2 u_1^N + \tau_1^N,$$
$$\left(\frac{\mu}{dt} + E \right) A_1 u_2^{N+1} = \frac{\mu}{dt} A_2 u_2^N + \tau_2^N, \tag{13}$$

with the matrix A_1 given by the following evolution matrix form:

$$\begin{bmatrix} \frac{2}{dx} + \frac{2}{dy} & \frac{-1}{dx} & 0 & \frac{-1}{dy} & 0 & \cdots & \cdots & \cdots & \cdots & 0 \\ \frac{-1}{dx} & \frac{2}{dx} + \frac{2}{dy} & \frac{-1}{dx} & 0 & \frac{-1}{dy} & \ddots & \vdots & \vdots & \vdots & \vdots \\ 0 & \frac{-1}{dx} & \ddots & 0 & 0 & 0 & \ddots & \vdots & \vdots & \vdots \\ \frac{-1}{dy} & 0 & 0 & \ddots & \frac{-1}{dx} & \ddots & \frac{-1}{dy} & \ddots & \vdots & \vdots \\ 0 & \frac{-1}{dy} & \ddots & \frac{-1}{dx} & \ddots & \frac{-1}{dx} & \ddots & \frac{-1}{dy} & \ddots & \vdots \\ \vdots & \ddots & 0 & \ddots & \frac{-1}{dx} & \ddots & 0 & \ddots & \ddots & 0 \\ \vdots & \vdots & \ddots & \frac{-1}{dy} & \ddots & 0 & \ddots & \ddots & \ddots & \frac{-1}{dy} \\ \vdots & \vdots & \vdots & \ddots & \frac{-1}{dy} & \ddots & \ddots & \ddots & \ddots & 0 \\ \vdots & \vdots & \vdots & \vdots & \ddots & \ddots & \ddots & \ddots & \ddots & \frac{-1}{dx} \\ 0 & \cdots & \cdots & \cdots & \cdots & \cdots & 0 & 0 & \frac{-1}{dx} & \frac{2}{dx} + \frac{2}{dy} \end{bmatrix}.$$

We simulated wound healing using systems derived for both one-dimensional and two-dimensional cases using the scientific programming language Scilab with the following parameters from the literature. In the one-dimensional case, we considered a line domain to represent damaged skin, whereas, in the two-dimensional, we considered a rectangular domain to represent damaged skin.

- $R = 0.2$
- $s = 1$,
- $\rho_i = 0.1$,
- $\mu = 1$,
- $\varepsilon = 0.01$,
- $E = 0.01$,
- $\tau = 0.1$.

4 Results

The following sections present and discuss the finding from solving the coupled system numerically. We will show the results in two parts: a two-dimensional case and a three-dimensional case.

4.1 Two-dimensional Case

The results from the simulation reveal that cell density recovers quickly following an injury to the skin (Fig. 1a). It can also be seen that cell density recovers fully, while the extracellular matrix takes a long time to recover, and in most cases, it never recovers fully (Fig. 1b). These results are consistent with what Murray and Oster [8] found from their model. The cells move rapidly into the wound, and gradually the movement of cells slows down (Fig. 2). The direction movement of cells is in response to a chemotactic stimulus. Each side of the cell forms adhesion to the substrate and engages in a tug-of-war. Net displacements happen in the direction of the side with the strongest pull and the firmest attachments to the substrate. Hence, the displacements in the middle of the wound are in the direction of the negative.
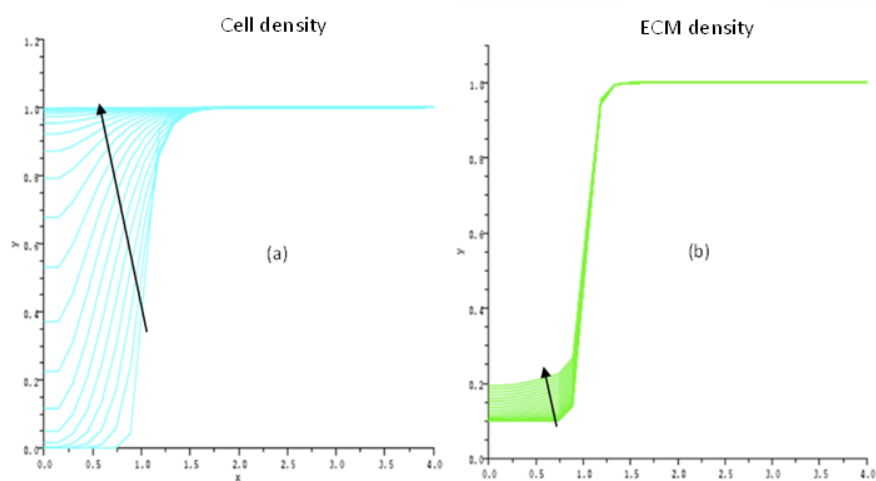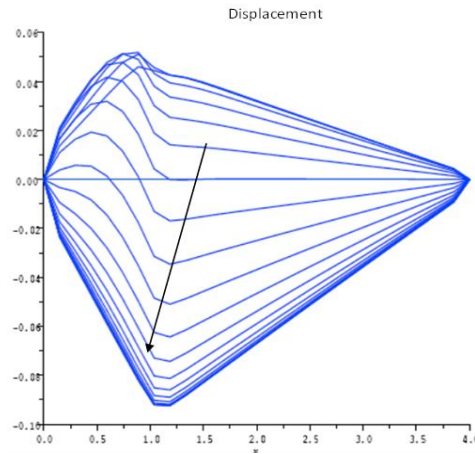

Fig. 1. Evolution of cell density (a) within the damaged wound and evolution of extracellular matrix (ECM) density (b) within during the wound healing. The arrow indicates how cell density or ECM density evolves with time during wound healing

4.2 Three-dimensional case

The same pattern observed in two dimensional is again observed in the three-dimensional: cell density recovers quickly (Fig. 3), but the ECM density still takes a long time to heal completely (Fig. 4). The red arrows show that the cell density and ECM density evolve with time during wound healing. The movement of cells is

dependent on the direction of flow; some cells move in the x-direction (Fig. 5a) and others in the y-direction (Fig. 5b) to replace the in cells. Again we observed that after the recovery of the injured, the movement of cells slowed down in both directions.

Fig. 2. displacements of cells to rapidly replace the dead cells during the wound healing. The arrow shows the direction of movement of cells with time during wound healing
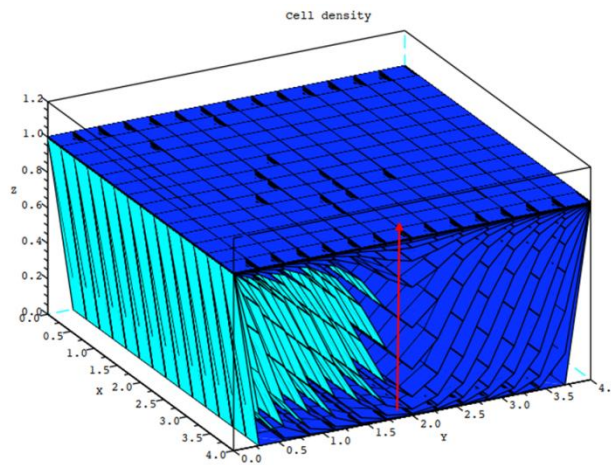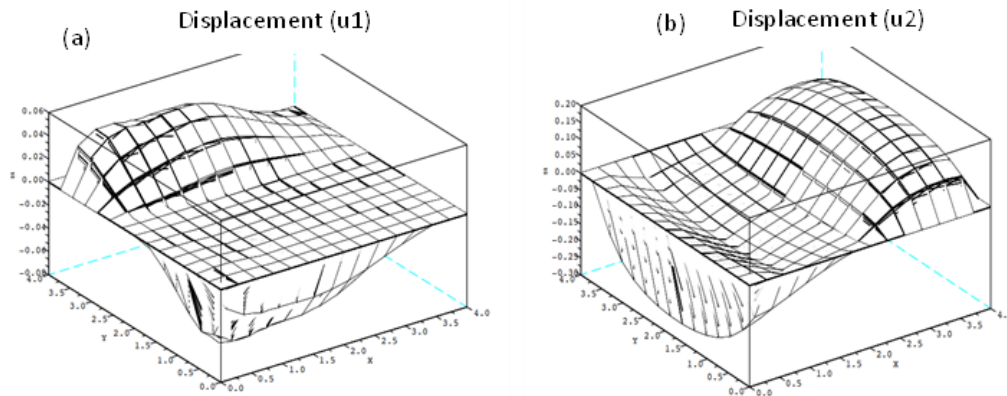

Fig. 3. Cell density evolution within the wound
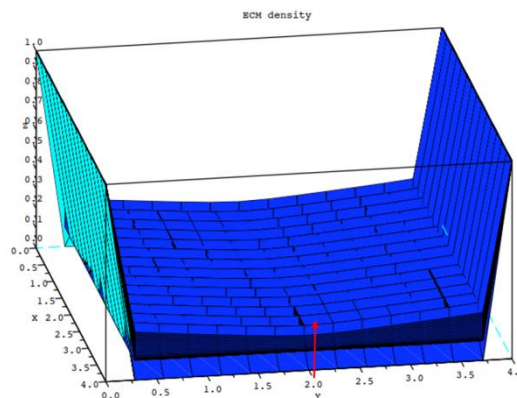
Fig. 4. ECM recovery during wound healing following the injured tissue. The red arrow indicates how slow the ECM is recovering with time

Fig. 5. The displacements of cells within the injured tissue during the healing process

5 Discussions

In this paper, we used the coupled reaction-diffusion, transport and viscoelastic system of partial differential equations to model wound healing in both two-dimensional and three-dimensional cases. We applied the implicit finite difference scheme with the Euler forward scheme for the time variable to discretize this coupled system of equations. During the discretization, attention was given to the flow direction during the cell migration within and around the wound domain. We took advantage of the stability of the implicit scheme. However, we ran into computational costs due to evolving sparse matrices and their inverses which had to be computed at each iteration.

The results from this simulation have shown that cell density returns to its normal functioning within a short time following the injury to the tissue. In contrast, the extracellular matrix takes a long time to return to its normal functioning state. The displacements of the cells have also shown that cells migrate fast from the normal tissue to the injured tissue. When the wound has returned to its close to a normal functioning state, the movement of cells has been shown to slow down.

6 Conclusions

This study can be extended to be applied to epithelial tissue injuries because it has been suggested that more than 90% of malignant tumours in adult mammalians occur in epithelial tissues. It is then of the highest importance to understand the dynamic regulations of focal adhesions involved during the cell migration in epithelial lines. This mathematical model can also be utilized to describe the closure behaviour from a pure kinematic point of view of a particular cell sheet, the Madin-Darby canine kidney (MDCK) monolayer cell sheet. But to do this, a global optimization algorithm needs to be performed to make parameter identification based on biological experiments. This computational tool developed will assist in shedding some original light on the mechanics which occur inside the cells sheet.

Competing Interests

Authors have declared that no competing interests exist.

References

[1]   Sherratt JA, Dallon JC. Theoretical models of wound healing: past successes and future challenges. Comptes Rendus Biologies. 2002;325(5):557-564.

[2]   Dale PD, Maini PK, Sherratt JA. Mathematical modeling of corneal epithelial wound healing. Mathematical biosciences. 1994;124(2):127-147.

[3]   Olsen L, Sherratt JA, Maini PK. A mechanochemical model for adult dermal wound contraction: on the permanence of the contracted tissue displacement profile. Journal of theoretical biology. 1995;177(2):113-128.

[4]   Sherratt JA, Murray JD. Models of epidermal wound healing. Proceedings of the Royal Society of London. Series B: Biological Sciences. 1990;241(1300):29-36.

[5]   Savakis A, Maggelakis S. Models of shrinking clusters with applications to epidermal wound healing. Mathematical and Computer Modelling. 1997;25(6):1-6.

[6]   Odland, G. and R. Ross, Human wound repair: I. Epidermal regeneration. The journal of cell biology. 1968;39(1):135-151.

[7]   McDougall S, Dalton J, Sherratt J, Maini P. Fibroblast migration and collagen deposition during dermal wound healing: mathematical modelling and clinical implications. Philosophical Transactions of the Royal Society of London A: Mathematical, Physical and Engineering Sciences. 2006;364(1843): 1385-1405.

[8]   Murray J, Oster G. Cell traction models for generating pattern and form in morphogenesis. Journal of mathematical biology. 1984;19(3):265-279.

[9]   Sherratt JA, Martin P, Murray JD, Lewis J. Mathematical models of wound healing in embryonic and adult epidermis. Mathematical Medicine and Biology: A Journal of the IMA. 1992;9(3):177-196.

[10]   Cumming BD, McElwain D, Upton Z. A mathematical model of wound healing and subsequent scarring. Journal of The Royal Society Interface. 2010;**7**(42):19-34.

[11]   Flegg JA, Shakti SN, Maini PK, Sean Mc Elawain DL. On the mathematical modeling of wound healing angiogenesis in skin as a reaction-transport process. Frontiers in physiology. 2015;6:262.

[12]   Jorgensen SN, Sanders JR. Mathematical models of wound healing and closure: a comprehensive review. Medical & biological engineering & computing. 2016;54(9):1297-1316.

[13]   Cerda E. Mechanics of scars. Journal of biomechanics. 2005;38(8):1598-1603.

[14]   Larrabee Jr, WF, Galt J. A finite element model of skin deformation. III. The finite element model. The Laryngoscope. 1986;96(4):413-419.

[15]   Maini PK, Olsen L, Sherratt JA. Mathematical models for cell-matrix interactions during dermal wound healing. International Journal of Bifurcation and Chaos. 2002;12(09):2021-2029.

[16]   Shoemaker P, Schneider D, Lee MC, Fung YC. A constitutive model for two-dimensional soft tissues and its application to experimental data. Journal of Biomechanics. 1986;19(9):695-702.

[17]   Guerra A, Belinha J, Jorge RN. Modelling skin wound healing angiogenesis: A review. Journal of theoretical biology. 2018;459:1-17.

[18]   Rouillard AD, Holmes JW. Mechanical regulation of fibroblast migration and collagen remodelling in healing myocardial infarcts. Journal of physiology. 2012;590(18):4585-4602.

[19]   Rouillard AD, Holmes JW. Coupled agent-based and finite-element models for predicting scar structure following myocardial infarction. Progress in biophysics and molecular biology. 2014;115(2):235-243.

[20]   Olsen L, Sherratt JA, Maini PK. A mathematical model for fibro-proliferative wound healing disorders. Bulletin of mathematical biology. 1996;58(4):787-808.

[21]   Olsen L, Sherratt JA, Maini PK, Anorld F. A mathematical model for the capillary endothelial cell-extracellular matrix interactions in wound-healing angiogenesis. Mathematical Medicine and Biology: A Journal of the IMA. 1997;14(4):261-281.

[22]   Gbenro SO, Nchejane JN. Numerical Simulation of the Dispersion of Pollutant in a Canal. Asian Research Journal of Mathematics. 2022;18(4):25-40.

[23]   Nchejane JN, Gbenro SO. Nonlinear Schrodinger Equations with Variable Coefficients: Numerical Integration. Journal of Advances in Mathematics and Computer Science. 2022;37(3):56-69.

_____

Peer-review history:
The peer review history for this paper can be accessed here (Please copy paste the total link in your browser address bar)
https://www.sdiarticle5.com/review-history/87715